Textures and Microstructures, 1996, Vol. 26–27, pp. 321–335
Reprints available directly from the publisher
Photocopying permitted by license only

ORIENTATION SELECTION DURING STATIC RECRYSTALLIZATION OF CROSS ROLLED NON-ORIENTED ELECTRICAL STEELS

L. KESTENS†, J. J. JONAS‡, P. VAN HOUTTE° and E. AERNOUDT°

†Department of Flat Rolling, Centrum voor Research in de Metallurgie, Technologiepark 9, B-9052 Gent, Belgium
‡Department of Metallurgical Engineering, McGill University, 3450 University Street, Montreal, Quebec, Canada, H3A 2A7
°Department of Metallurgy and Materials Engineering, Katholieke Universiteit Leuven, de Croylaan 2, B-3001 Leuven, Belgium

(Received 14 February 1996)

Very sharp deformation textures, with single maxima of more than 50x random centred on the rotated cube component ({001}<110>), were produced by submitting a non-oriented electrical steel sheet to various sequences of cross-rolling. The cold rolled sheets were subsequently annealed at 730°C for 3 min. The resulting recrystallization textures were much weaker than the cold rolling textures, displaying maxima of about 5x random at locations some distance away from the {001}<110> cross rolling component.

Due to the very sharp character of the rolling texture, the conventional low and high stored energy nucleation mechanisms were effectively prevented from operating. Thus orientation selection could only take place by the selective growth of nuclei external to the dominant rolling component. Quantitative analysis of the experimental ODFs revealed that the rolling and recrystallization components are related by Σ27 (31.6°<110>) and Σ7c (38.2°<111>) coincidence site lattice (CSL) orientation relations. Simulations of the annealing texture on the basis of random nucleation and combined Σ27-Σ7c selective growth produced reasonable agreement between the predictions and the experimental results.

KEY WORDS: Electrical steel, cross-rolling, non-oriented, recrystallization texture, orientation selection, mathematical model.

INTRODUCTION

Our current understanding of the mechanism of orientation selection during the annealing of commercial steels is based on the analysis of two successful types of texture control. The first and most obvious example involves the development of grain oriented electrical steels with their excellent magnetic properties for transformer applications (Takahashi and Harase, 1995). These steels possess very strong Goss ({110}<001>) textures in which the average deviation of the <100> crystallographic direction from the RD axis of the sheet is less than 3°.

The second well known example of texture control concerns the processing of deep drawing steels so as to produce sharp ND fibres (<111>//ND) in the annealed condition (Hutchinson, 1984). Particular interest has been paid in this case to the continuous annealing behaviour of IF (interstitial free) steels (Hutchinson, 1994). For these grades, the rolling texture prior to annealing invariably contains two components: i) the ND

fibre defined above, together with ii) the RD fibre (<110>//RD). These components are generated by conventional cold rolling (with reductions of 70% to 85%) carried out on hot bands with an austenite transformation texture. After recrystallization, this two-fibre texture is transformed into a single ND fibre texture, which may (or may not) be characterized by a distinct maximum somewhere along the fibre.

The appearance of the ND fibre orientations is commonly attributed to the oriented nucleation of high stored energy orientations in the deformed matrix (Hutchinson, 1992). The operation of this mechanism is supported by experimental observations (Vanderschueren *et al.*, 1996) as well as by recently developed computer models (Kestens and Jonas, 1996). There is still considerable debate, however, regarding the importance of selective growth, and in particular about the possible orientation dependence of grain boundary mobility under industrial conditions of annealing.

Experimental data supporting the view that selective growth occurs in polycrystalline bcc materials are scarce and circumstantial (Humphreys and Hatherly, 1995). The orientation relationship most commonly referred to as associated with increased mobility in the bcc lattice is 27° <110>. However, by means of recrystallization experiments on Fe-3% Si *single* crystals, Ibe and Lücke (1968) obtained evidence for the high mobility of boundaries associated with this particular misorientation, which can also be described as a Σ19a coincidence site lattice (CSL) misorientation. Other authors (Hölscher *et al.*, 1991; Urabe and Jonas, 1994; Köhler and Bunge, 1995) have argued that the 27° <110> orientation relation could be responsible for the frequently observed maximum centred on or near the {111}<211> component in annealed IF steels, since there exists a near 27°<110> orientation relationship between this orientation and the high intensity {211}<110> component of the rolling texture. Thus, according to Kestens and Jonas (1996), such oriented growth complements the occurrence of oriented nucleation mentioned above, and more significantly, accounts for some of the morphological features of observed recrystallization textures that cannot be explained exclusively on the basis of an oriented nucleation theory.

Some observations by Inagaki (1987a) and Yoshinaga *et al.* (1994) regarding a cold rolling texture consisting exclusively of an ND fibre are of interest in this regard. Here the {111}<211> maximum, characteristic of the deformed material, was transformed into a {111}<110> maximum after recrystallization. Since no RD fibre orientations were present in the rolling texture in this experiment, the appearance of the {111}<110> component cannot be attributed to <110> selective growth. The initial and final orientations have a <111> common axis in this case. However, the increased mobility of bcc grain boundaries with common <111> axes has not been treated in any detail to date.

In the present paper, the results of some rolling and annealing experiments are described that were carried out in order to assess the relative importance of the nucleation and growth mechanisms described above. Of particular importance is the possible occurrence of <110> or <111> selective growth. It was assumed that certain features of orientation selection during annealing could be clarified by causing recrystallization to take place in rolling textures that differ considerably from the ones that are usually present in this type of experiment. Three contrasting sets of rolling conditions were employed, in each of which the cold rolling direction (CRD) was varied in a different way with respect to the hot rolling direction (HRD). By means of the altered rolling paths, textures were created that appreciably differed from the conventional rolling textures observed in low and extra-low carbon steels. The use of these unusual initial textures made it possible to isolate the role of selective growth more thoroughly than when the commonly observed rolling textures are involved.

EXPERIMENTAL

The cold rolling and annealing experiments were carried out on a commercially hot rolled non-oriented electrical steel. The composition, shown in Table 1, is typical for the lower grades of non-oriented electrical steel. Alloying elements, such as Si, Al and Mn, are added in order to increase the resistivity of the material as well as to improve the texture and therefore the magnetic properties.

The processing steps employed to prepare the three types of material are illustrated schematically in Figure 1. The three types of sample (A, B and C) were cut from the as-received hot rolled sheet and cold rolled on a laboratory mill in 11 successive passes. All the samples were submitted to an accumulated reduction of 70% (a true strain $\varepsilon = 1.2$); however, the rolling paths were different for each type of specimen. The sample A material was entirely cold rolled along a direction perpendicular to the previous hot rolling direction (CRD $\perp$ HRD). The sample B material was cold rolled in two stages of equal accumulated true strain ($\varepsilon = 0.6$). In the first stage, the CRD was parallel to the HRD and in the second stage, it was perpendicular to the HRD. During the preparation of the sample C material, specimens were rotated by 90° between successive passes.

After cold reduction, each material was given an annealing treatment in a salt bath at 730°C for 180 s. This temperature is considerably below the measured A_{r1} of 810°C, so that the samples were fully ferritic during annealing. In preliminary experiments (Kestens, 1994), it was established that an annealing time of 3 min. at 730°C is sufficient to produce a fully recrystallized structure.

After each processing step, the microstructures were evaluated by optical metallography. Four incomplete pole figures ({110}, {200}, {211} and {310}) were measured on a Siemens D500 texture goniometer. The ODFs were then calculated from these pole figures using the software developed by Van Houtte (1992).

RESULTS

Because most of the common rolling and recrystallization components found in bcc materials are located in the $\varphi_2 = 45°$ section of Euler space (cf. Figure 2), this representation will be used here to compare the textures of the different samples. For the cases that differ significantly from conventional bcc textures, however, the full ODF will be employed.

The texture of the hot rolled material is displayed in Figure 3a. It features a partial RD fibre (<110>//RD) with a sharp maximum of 26x random at the rotated cube component ({001}<110>). When a sample is cross cold rolled, it is rotated by 90° around the ND; thus the hot rolling direction is converted into the transverse cold rolling direction, while the transverse hot rolling direction is transformed into the cold rolling

Table 1 Composition of the non-oriented electrical steel (mass%).

C	*Mn*	*Si*	*P*	*S*	N_2	Al_{met}
0.036	0.153	0.575	0.010	0.004	0.0043	0.292

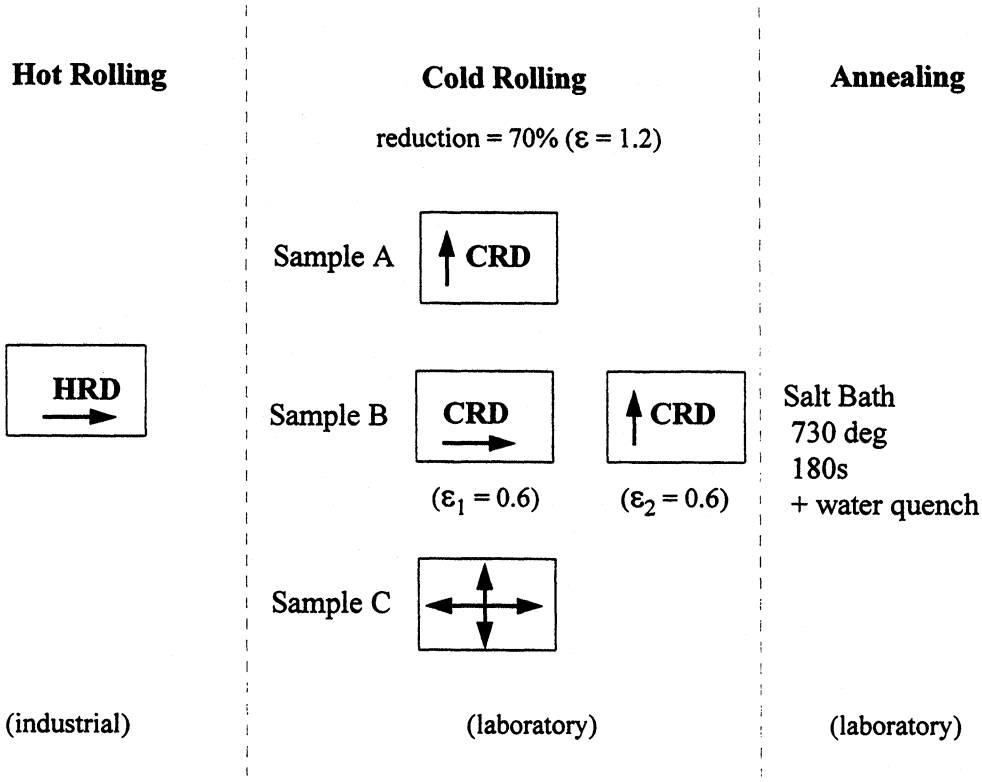

Figure 1 Schematic representation of the rolling sequences employed in the preparation of the A, B and C samples (HRD = hot rolling direction; CRD = cold rolling direction).

direction. The manner in which this change of sample reference system affects the $\varphi_2 = 45°$ section of the ODF is illustrated in Figure 3b. The rotation transforms the partial RD fibre into a partial TD fibre (<110>//TD). The latter is known to contain orientations that are much less stable during rolling than those belonging to the RD fibre (Tòth *et al.*, 1990).

The cold rolling textures of samples A, B and C are shown in Figures 4a, b and c, respectively. It can be seen that, irrespective of the details of the rolling path, all the samples exhibit a very sharp maximum at the rotated cube component. Only the strengths of the maxima vary from somewhat less than 50x for sample B to more than 150 for sample A. The intensity values of these very sharp maxima are dependent, however, on the method of pole figure inversion and ghost correction employed in the calculation of the ODF. The values are therefore subject to error and should be considered instead to give qualitative indications of unique and very strong maxima centred on {001}<110>.

The striking similarity that applies to the rolling textures of the A, B and C samples also extends to the annealing textures, as can be seen in Figures 5a, b and c, respectively.

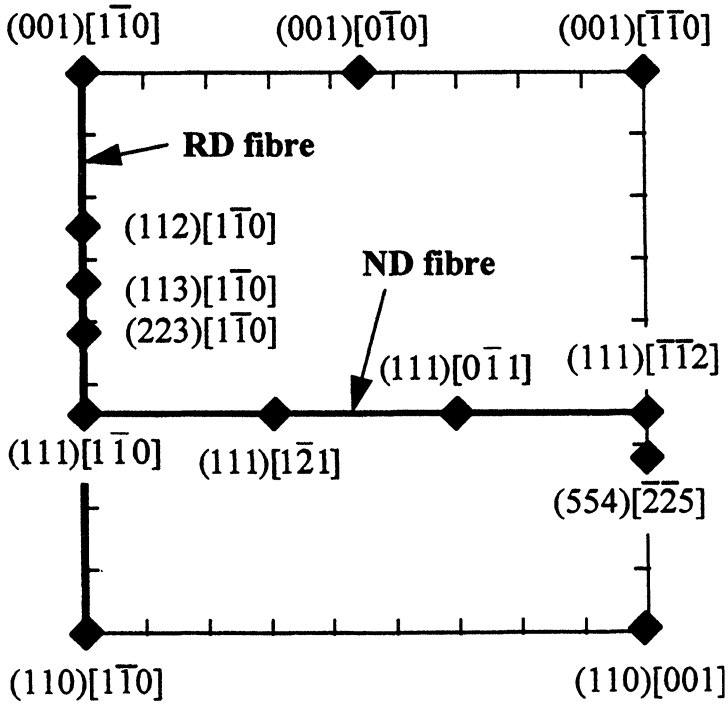

Figure 2 $\varphi_2 = 45°$ section of Euler space showing the ideal bcc rolling and recrystallization texture components.

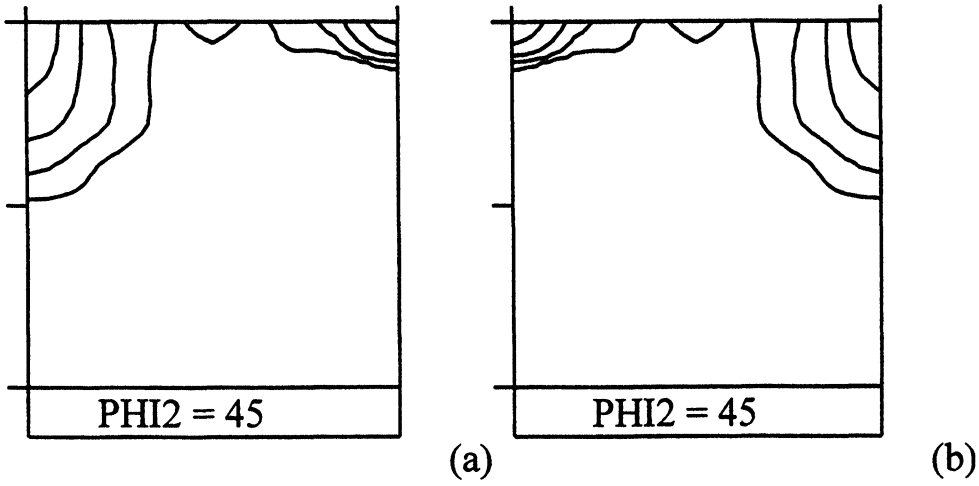

Figure 3 (a) Hot rolling texture (max 25.8) and (b) hot rolling texture presented in the cross-rolling reference frame (rotated by 90°). Iso-levels: 2–4–8–16.

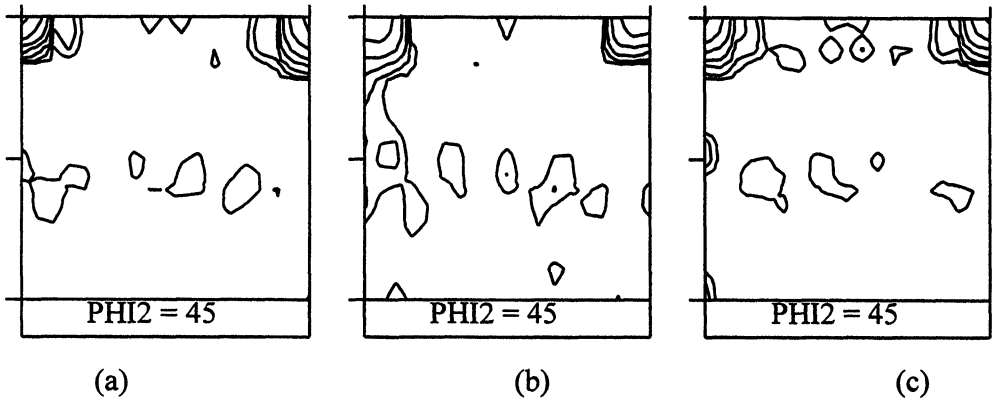

Figure 4 Cold rolling texture (a) sample A (max 156.1), (b) sample B (max. = 49.6) and (c) sample C (max. = 133.0). In all cases, the sample reference system corresponds to that of the hot rolled sample. Iso-levels: 2–4–8–16–32–64–128.

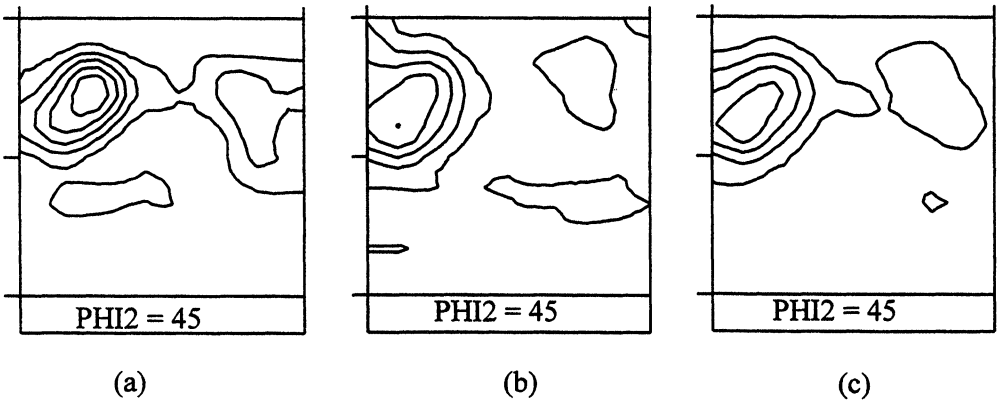

Figure 5 Annealing textures (a) sample A (max 6.8), (b) sample B (max. = 5.1) and (c) sample C (max. = 5.0). In all cases, the sample reference system corresponds to that of the hot rolled sample. Iso-levels: 1–2–3–4–5–6.

It should be noted, however, that these recrystallization textures stand in sharp contrast to the commonly observed annealing textures of conventionally rolled sheets (Ray *et al.*, 1994). As a result, the present ODFs can no longer be adequately characterized by single $\varphi_2 = 45°$ sections. The full ODF of the material subjected to two-stage rolling (sample B) is therefore presented in Figure 6. (Here φ_1 = constant and $\varphi_2 = 45°$ sections are employed for convenience.) Because of the similarities between the annealing textures of all the samples, Figure 6 can be regarded as representative of this entire class of texture.

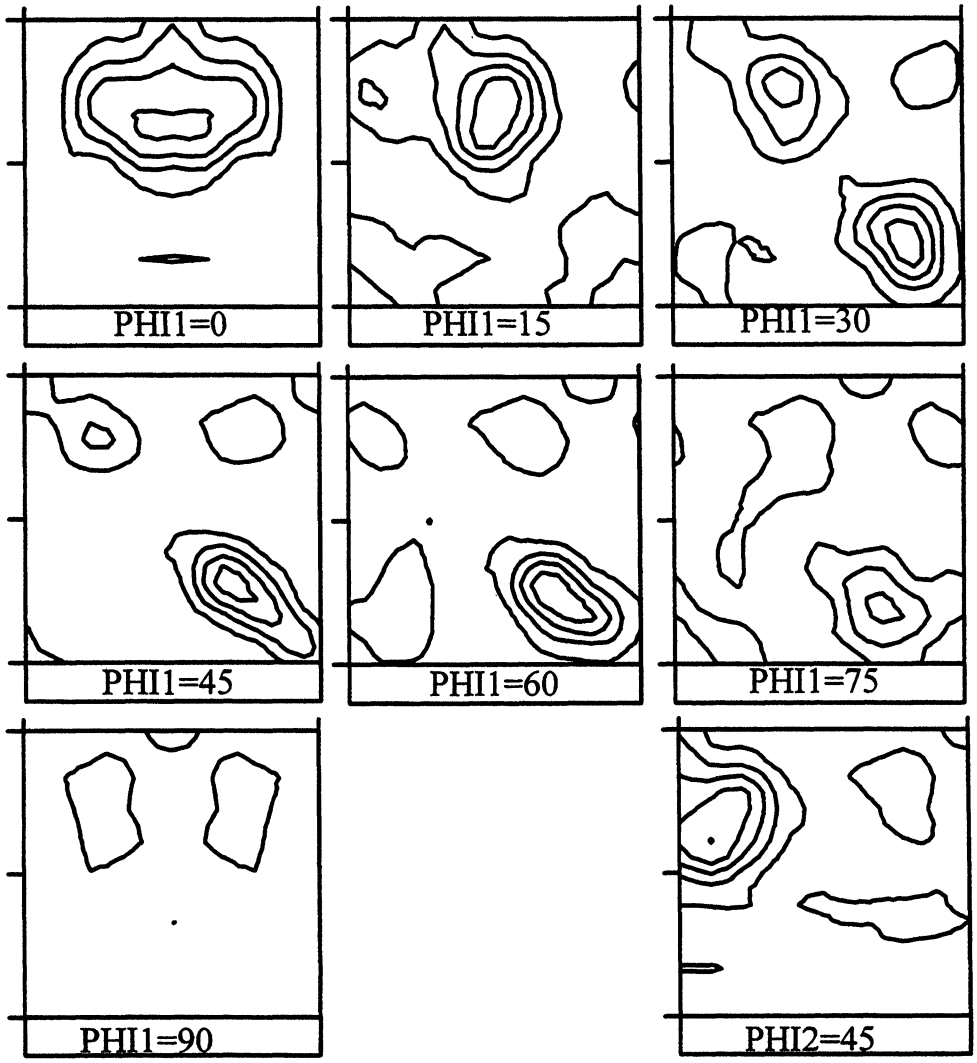

Figure 6 Full ODF of the annealed sample prepared by two-stage cold rolling (sample B) (φ_1 = constant + φ_2 = 45° sections). Iso-levels: 1–2–3–4–5–6.

The location of the point of maximum intensity in the recrystallization ODFs of these materials is listed in Table 2 as a set of Euler angles. Also shown are the orientation distances to the nearest recrystallization variants that can be described in terms of CSL rotations about a common <110> or <111> axis. (Here the "origin" for each rotation is the observed intensity maximum located at {001}<110> in each of the cross-rolled materials, see Figure 5.) From these data it can be seen that the orientation relation that applies to the rolling and recrystallization maxima in samples B and C is 10.8°

Table 2 Orientation distances between the intensity maxima pertaining to the experimental annealing textures and the nearest ideal CSL positions.

Sample	*ODF max* (φ_1,Φ,φ_2)	*CSL* ω°<*uvw*>	*Distance (deg)*	*Sample*	*ODF max* (φ_1,Φ,φ_2)	*CSL* ω°<*uvw*>	*Distance (deg)*
B,C	40,65,65	Σ33a 20<110>	17.8	A	15,25,55	Σ33a 20<110>	20.3
		Σ19a 27<110>	13.2			Σ19a 27<110>	17.7
		Σ27 32<110>	10.8			Σ27 32<110>	17.4
		Σ9 39<110>	11.0			Σ9 39<110>	19.1
		Σ11 51<110>	18.7			Σ11 51<110>	26.1
		Σ17c 87<111>	25.8			Σ17c 87<111>	55.3
		Σ21a 22<111>	17.2			Σ21a 22<111>	14.1
		Σ13b 28<111>	13.4			Σ13b 28<111>	8.9
		Σ7c 38<111>	12.2			Σ7c 38<111>	6.5
		Σ19b 47<111>	16.9			Σ19b 47<111>	13.2

away from an exact Σ27 31.6° <110> CSL and 12.2° away from an exact Σ7c 38.2° <111> CSL. In sample A, the nearest exact CSL orientation relation is Σ7c, which is 6.5° away from the observed misorientation.

DISCUSSION

The Cold Rolling Textures

Although the rolling textures of the three different samples differ somewhat in the low intensity regions of Euler space, they are similar to a first approximation. The most characteristic feature is the sharp maximum centred on the rotated cube component {001}<110>, an observation that applies to all the rolling paths. This component, with its tetragonal symmetry (x_3 = 4-fold symmetry axis), is stable with respect to both directions of rolling. Similar conclusions regarding the appearance of this orientation after cross rolling were drawn by Böcker *et al.* (1990).

In order to analyse the deformation ODFs, the evolution of the texture was simulated using the various full and relaxed constraint plasticity models developed by Van Houtte (1988). Following the approach of Daniel and Jonas (1990), the critical resolved shear

stress ratio for {211} slip relative to {110} slip was set equal to 0.95. The rolling textures simulated on the basis of a relaxed constraint pancake model are illustrated in Figures 7a, b and c. (E_{13} and E_{23} are the relaxed components of the deformation tensor, where the rolling, transverse and normal directions are 1, 2 and 3, respectively). It can be seen that the simulations pertaining to the three types of sample are in good agreement with the measured rolling textures of Figures 4a, b and c, respectively. Nevertheless, the {111}<110> minority component is slightly overestimated in the predictions. Had the full constraint theory been employed instead of the pancake model, however, the intensity of this component would have been somewhat greater.

A detailed quantitative comparison between the model predictions and the experimental results is highly questionable for this type of very sharp texture, as the intensity maxima depend sensitively on technical parameters such as the degree of the series expansion of the ODF, the number of discrete orientations employed in the simulation, and the Gaussian spread around each orientation used to produce the final ODF. For this reason, the agreement between Figures 4 and 7 is, in fact, highly satisfactory.

The Recrystallization Textures

It was suggested in an earlier paper (Kestens, *et al.*, 1996) that a powerful randomization mechanism operates during the recrystallization of this particular type of non-oriented electrical steel. In fact, hot band processing favours the precipitation of coarse particles (cementite, nitrides, sulfides and phosphides) in the hot rolled sheet, as reported by De Paepe *et al.* (1995). Such coarse particles are often associated with particle stimulated nucleation PSN (Humphreys, 1977), which is in turn reported to give rise to randomly oriented nuclei (Inagaki, 1987b).

Even if PSN is not taking place in the present material, it remains likely that only randomly oriented nuclei are able to grow. Given the very sharp maximum centred on the rotated cube component in the rolling texture, this component could be expected to dominate the nucleation texture, whatever the mechanism of oriented nucleation.

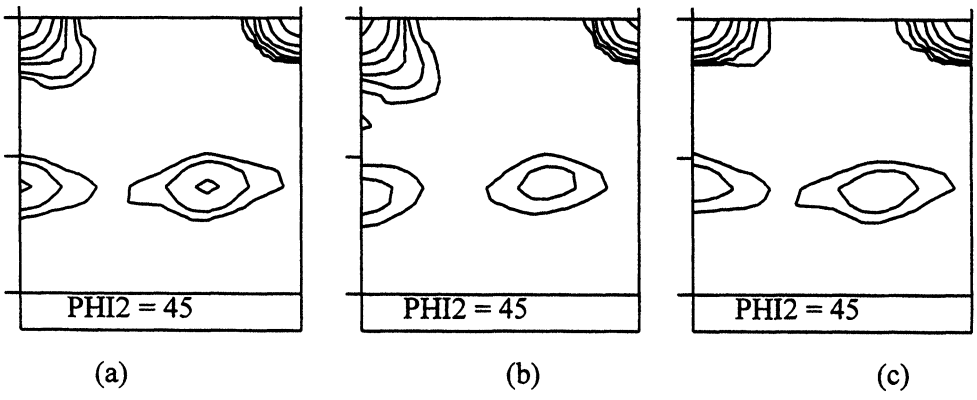

Figure 7 Simulated rolling textures calculated using the relaxed constrains (pancake) method: (a) sample A (max. 120.7), (b) sample B (max. 88.1) and (c) sample C (max. 145.4). Iso-levels: 2–4–8–16–32–64–128.

However, {001}<110> nuclei are likely to grow only slowly in the {001}<110> matrix because of the restricted mobility of low angle grain boundaries. Thus only nuclei situated more than say 15° away from {001}<110>, that is in the remainder of the matrix, have a real potential for growth.

The observed recrystallization textures indicate that such growth does indeed occur. However, not *all* high angle grain boundaries migrate at the same rate because some are more mobile than others. This leads to distinct growth competition, which is why peaks appear in the annealing textures at locations that differ distinctly from those associated with the deformation texture. The data of Table 2 suggest that such selective growth is indeed taking place, and that Σ27 and Σ7c rotations play predominant roles in this process. In order to evaluate the possible role of these CSL relationships, the {001}<110> rolling component was transformed into the twelve 31.6°<110> variants (these include both positive and negative rotations about the six <110> axes) and the eight 38.2°<111> variants (positive and negative rotations about the four <111> axes). The results of these transformations are presented in the ODFs of Figures 8 and 9, respectively. Each of these textures bears a reasonable resemblance to the measured texture of Figure 6, although significant differences remain.

A more quantitative means of comparing the model predictions with the experimental textures involves calculating the index I associated with the difference ODF that pertains to the measured (f_{exp}) and calculated (f_{mod}) ODFs.

$$I = \int_{\Omega} (f_{exp} - f_{mod})^2 \, dg \qquad [1]$$

with the integral extending over the total volume Ω of Euler space.

The value of I derived from the measured and predicted annealing textures are listed in Table 3 for samples A, B and C. Here the rolling textures were transformed according to the 31.6°<110> ($f_{mod} = f_{\Sigma 27}$) and 38.2°<111> ($f_{mod} = f_{\Sigma 7c}$) relations described above. It should be noted that the <111> rotation leads to a significantly better fit than the <110> rotation for sample A. Nevertheless, given the approximately equal deviations from the observed textures displayed by the 31.6°<110> and 38.2°<111> rotations, the view was adopted here that both types of CSL boundary are active concurrently during selective growth. The model ODF of Figure 10 was then calculated on the basis of this dual mode of growth selection. For this purpose, the model ODFs of Figure 8 and 9 were simply merged. When this merged ODF was compared with the experimental one, employing the texture index applicable to the difference ODF, the

Table 3 Texture indices (I) associated with difference ODFs linking the simulated (f_{mod}) and experimental (f_{exp}) textures.

f_{exp}	f_{mod}	I
Sample A	$f_{\Sigma 7c}$	1.216
Sample A	$f_{\Sigma 27}$	1.113
Sample B	$f_{\Sigma 7c}$	0.727
Sample B	$f_{\Sigma 27}$	1.393
Sample C	$f_{\Sigma 7c}$	1.002
Sample C	$f_{\Sigma 27}$	0.951

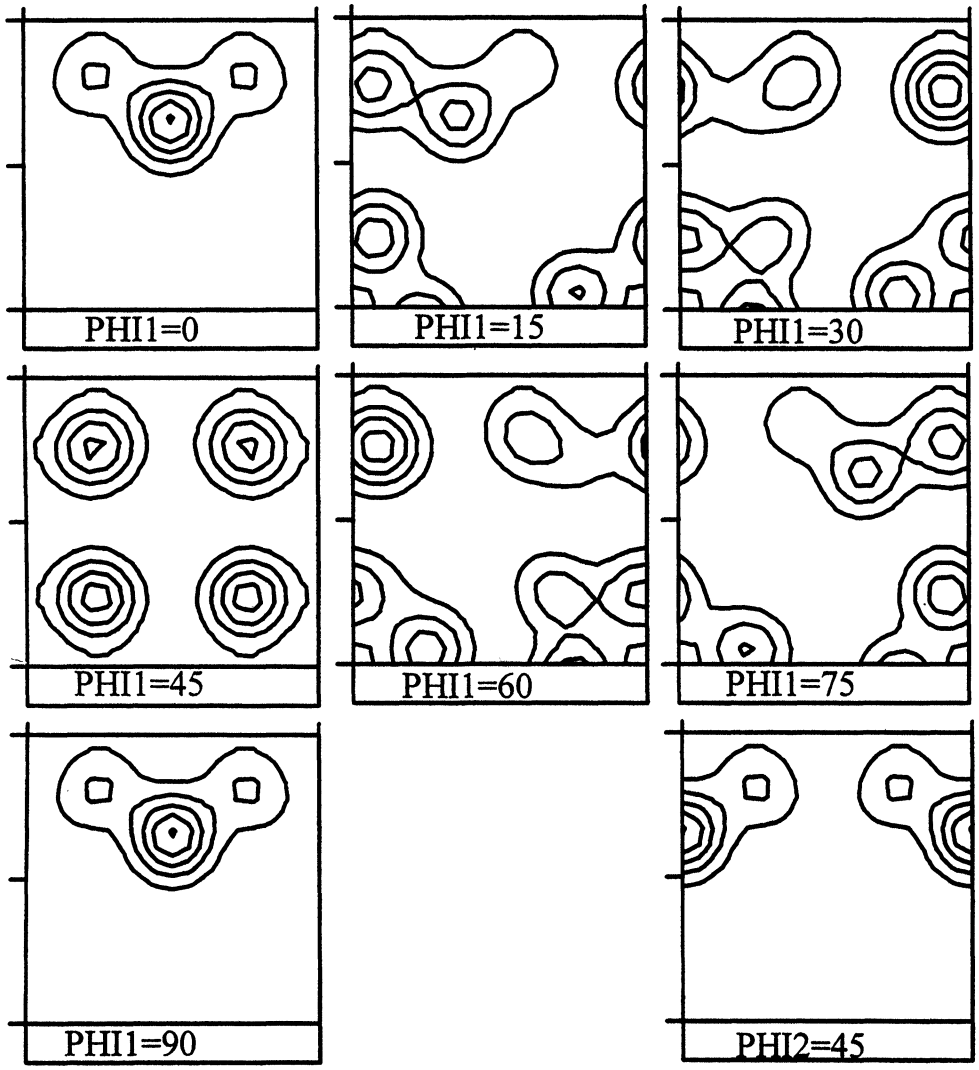

Figure 8 Simulation ODF obtained by transforming the {001}<110> component using the Σ27 31.6° <110> CSL relationship. Iso-levels: 1–2–3–4–5–6.

following values were obtained for samples A, B and C respectively: 0.535, 0.431 and 0.347. The significant reduction in the I values brought about in this way (compared to the values in Table 3) leads support to the hypothesis that both kinds of selective growth are taking place.

Despite the fairly good agreement obtained by assuming that a dual form of Σ7c-Σ27 selective growth takes place, there remains an important discrepancy between the experimental and measured ODFs. Although all the major components of the measured texture are present in the model texture of Figure 10, the reverse relationship does

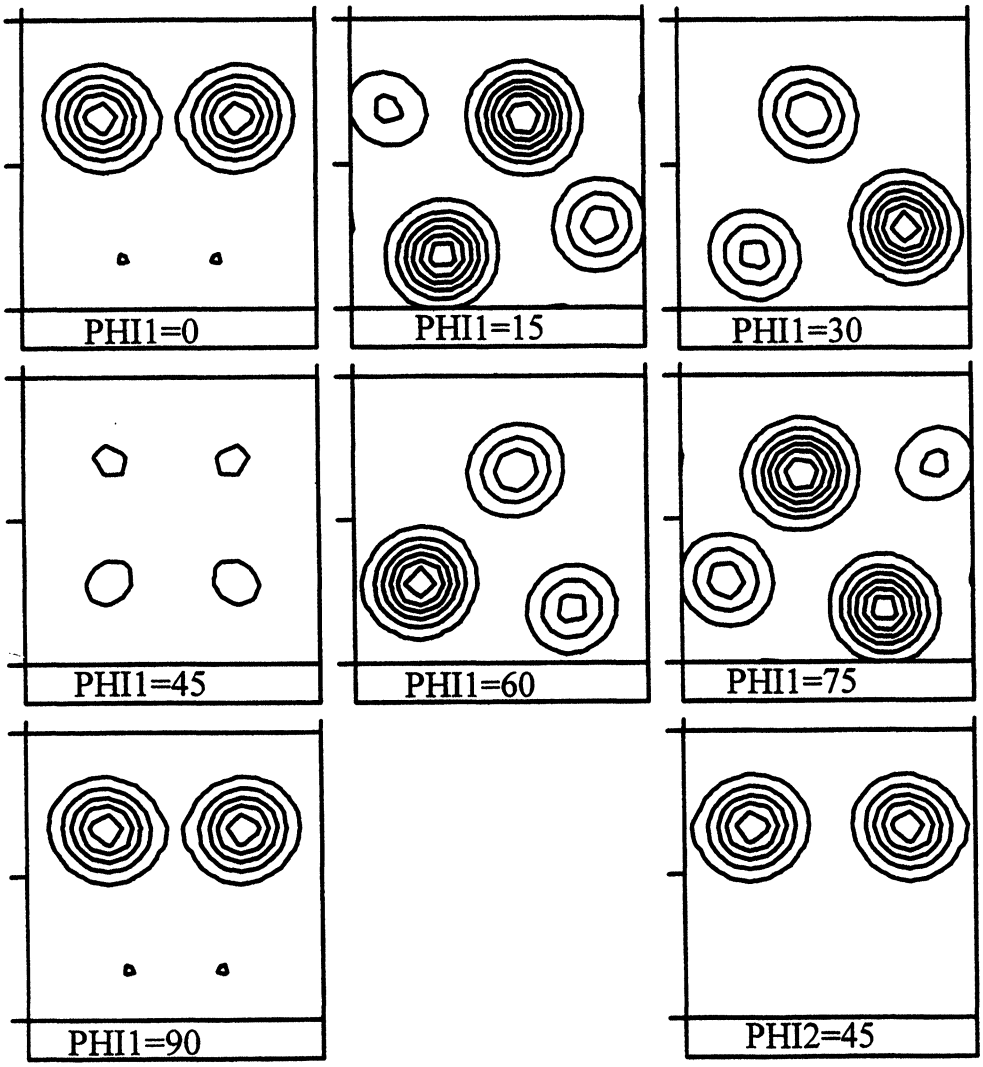

Figure 9 Simulation ODF obtained by transforming the {001}<110> component using the Σ7c 38.2° <111> CSL relationship. Iso-levels: 1–2–3–4–5–6–7.

not hold. This suggests that some form of variant selection is occurring or that a certain amount of oriented nucleation is taking place. It is of interest to note that orientations in regions along the <110>//HRD fibre that were already densely populated in the hot rolling texture are also more intense in the $\varphi_2 = 45°$ section of the annealing texture. This indicates that the annealing texture is influenced by the morphology of the hot rolling texture. A similar effect is observed in the low intensity areas of the cold rolling texture that have higher intensities in the vicinity of the <110>//HRD fibre (cf. Figure 4b).

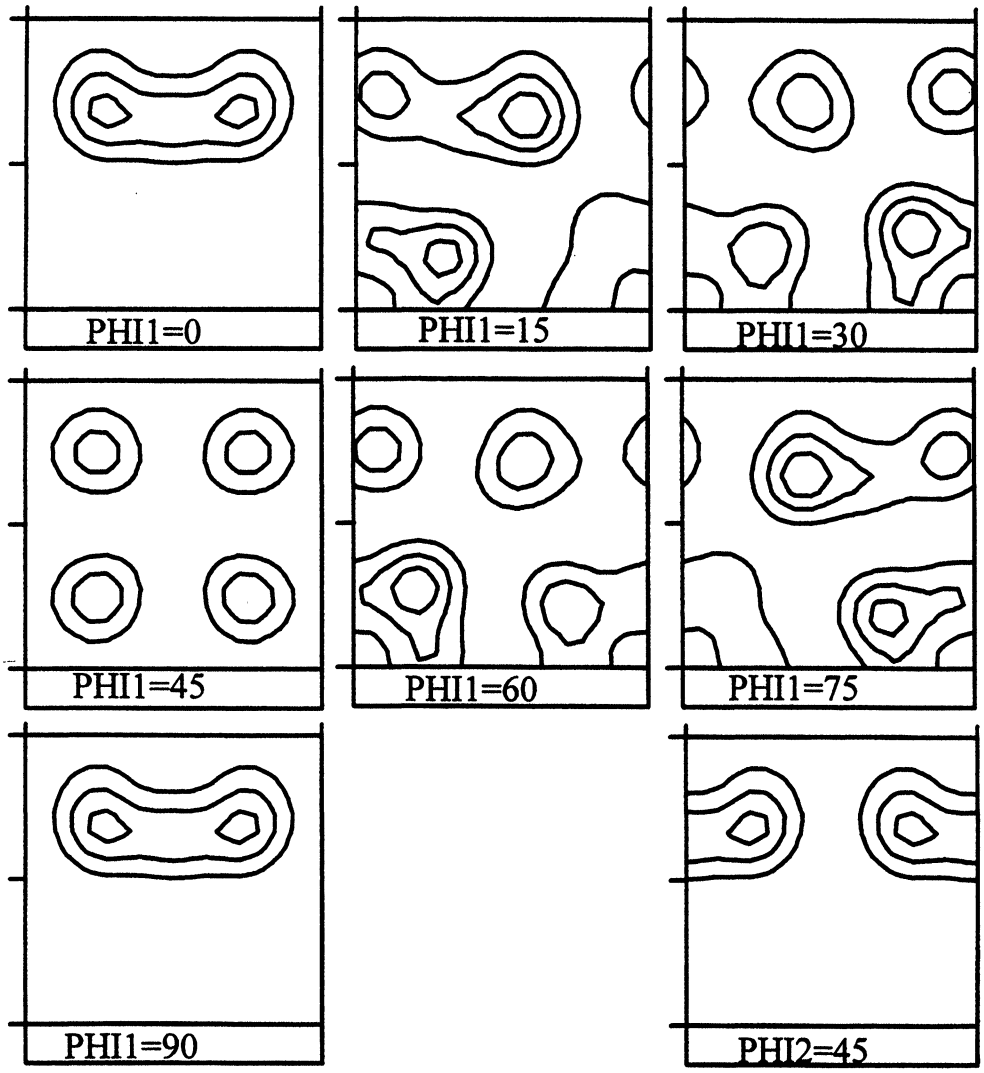

Figure 10 Simulation ODF obtained by summing the ODFs displayed in Figure 8 and 9. Iso-levels: 1-2-3.

SUMMARY AND CONCLUSIONS

A hot rolled sheet of a non-oriented electrical steel was submitted to various sequences of cross rolling. In this way, the initial strong hot band texture was concentrated into a single component cold rolling texture with a very sharp maximum centred on the rotated cube component ({001}<110>).

After recrystallization, a comparatively weak annealing texture appeared in which the observed maxima were shifted significantly away from the {001}<110> rolling component. The recrystallization textures were similar, despite the rolling path differences and thus the deformation substructures differences. This illustrates that the input deformation texture plays a larger role than the substructure in determining the output annealing texture.

By effectively preventing conventional high or low stored energy nucleation from taking place, the present experimental procedure made it possible to probe into the role of selective growth. A detailed quantitative analysis revealed that the rolling and recrystallization components were related by near 32° <110>(Σ27) and 38° <111>(Σ7c) orientation relationships. The recrystallized textures modelled on the basis of random nucleation and combined Σ27-Σ7c selective growth display satisfactory agreement with the observed annealing textures.

Acknowledgments

The authors are indebted to the N. V. Sidmar Steel Corporation, Belgium for providing the samples for this work and to the Belgian programme on Interuniversity Poles of Attraction initiated by the Belgian state, Prime Minister's office, Science Policy Programming. The authors express their appreciation to Ir. Ch. Standaert and Dr. D. Vanderschueren of the OCAS Research Centre, Belgium as well as to Dr. K. Eloot and Prof. J. Dilewijns of the Ghent State University, Belgium for numerous helpful discussions. The fruitful correspondence with Dr. U. Köhler of Technische Universität Clausthal is gratefully acknowledged. Thanks are also due to Dr. J. Savoie for his assistance with the Texture Menu software developed at McGill University.

References

Böcker A., Klein H. and Bunge H. -J. (1990). Development of cross-rolling textures in Armco-iron. *Text. and Micr.*, **12**, 103–123.

Daniel D. and Jonas J. J. (1990). Measurement and prediction of plastic anisotropy in deep-drawing steels. *Met. Trans. A*, **21A**, 331–343.

De Paepe A., Eloot K., Dilewijns, J. and Standaert C. (1995). Effect of hot rolling parameters on the magnetic properties of a low-silicon ultra low-carbon steel. Paper presented at *SMM 12*, September 1995, Krakow, Poland, to be published to *Journ. Magn. and Magn. Mat.*

Hölscher M., Raabe D. and Lücke K. (1991). Rolling and recrystallization textures of BCC steels. *Steel Research*, **62**, 567–575.

Humphreys F. J. (1977). The nucleation of recrystallization at second phase particles in deformed aluminium. *Acta Metall.*, **25**, 1323–1344.

Humphreys F. J. and Hatherly M. (1995). The mobility and migration of boundaries in *Recrystallization and Related Annealing Phenomena*, pp. 85–120, Oxford: Elsevier Science Ltd.

Hutchinson W. B. (1984). Development and control of annealing textures in low-carbon steels. *Int. Metall. Rev*, **29**, 25–42.

Hutchinson W. B. (1992). Nucleation of recrystallization. *Scripta. Met.*, **27**, 1471–1475.

Hutchinson W. B. (1994). Evolution of texture and anisotropy during recrystallization of IF steels. in. *Int. Forum for Physical Metallurgy of IF Steels*, edited by Iron and Steel Inst. of Japan, pp. 127–140, Tokyo.

Ibe G. and Lücke K. (1968). Orientierungszusammenhänge bei der Rekristallisation von Ein-kristallen einer Eisen-Silizium-Legierung mit 3% Si. *Archiv für das Eisenhüttenwese*, **39**, 693–703.

Inagaki H. (1987a). Stable end orientations in the rolling textures of the polycrystalline iron. *Z. Metallkunde*, **78**, 431–439.

Inagaki H. (1987b). Cracking of cementite particles and its influences on the development of the rolling texture in low carbon steels. *Z. Metallkunde*, **78**, 630–638.

Kestens, L. (1994). Oriëntatie-selektieve rekristallisatie in staalplaat voor elektromotoren, *PhD thesis*, pp. 72–73, Leuven: Catholic University of Leuven, (in Dutch).

Kestens L. and Jonas J. J. (1996). Modelling texture change during the static recrystallization of IF steels. *Metall. and Mater. Trans.*, **27A**, 155–164.

Kestens L., Jonas J. J., Van Houtte P. and Aernoudt E. (1996). Orientation selective recrystallization of non-oriented electrical steels, *Metall. and Mater. Trans.*, in press.

Köhler U. and Bunge H. J. (1995). Model calculations of the recrystallization texture formation in α-iron. *Text. and Micr*, **23**, 87–114.

Ray R. K., Jonas J. J. and Hook R. E. (1994). Cold rolling and annealing textures in low carbon and extra low carbon steels. *Int. Mater. Rev*, **39**, 129–172.

Takahashi N. and Harase J. (1995). The role of grain boundary character distribution in Goss texture development in electrical steels, presented at *Second International Conference on Grain Growth (ICGG-2)*, Kitakyushu, Japan, May 1995, in press.

Tòth L. S., Jonas J. J., Daniel D. and Ray R. K. (1990). Ferrite rolling textures in low and textra low carbon steels. *Metall. Trans. A*, **21A**, 2985–3000.

Urabe, T. and Jonas J. J. (1994). Modeling texture change during the recrystallization of an IF Steel. *ISIJ Int.*, **34**, 435–442.

Van Houtte P. (1988). A comprehensive mathematical formulation of an extended Taylor-Bishop-Hill model featuring relaxed constraints, the Renouard-Wintenberger theory and a strain rate sensitivity model. *Text. and Micr.*, **8–9**, 313–340.

Van Houtte P. (1992). The MTM-FHM software system, Release 1, August 1992, Personal Communication.

Vanderschueren D., Yoshinaga N. and Koyama K. (1996), Recrystallisation of Ti IF steel investigated with EBSP, *ISIJ Int.*, **36**, in press.

Yoshinaga N., Vanderschueren D., Oyama K., Ushioda K. (1994), Recrystallisation behavior of electrolytically deposited pure iron. *CAMP-ISIJ.*, **7**, 1692.